MSEC2024-XXXXX

INVESTIGATING THE EFFECT OF ALIGNED MICROTUBE DENSITY ON THE MECHANICAL

Texas Tech University Lubbock, TX

ABSTRACT

Tissue engineering is a pivotal research domain, central to advancing biomedical manufacturing processes with the aim of fabricating functional artificial organs and tissues. Addressing the pressing concern of organ shortages and myriad medical challenges necessitates innovative manufacturing techniques. Hydrogel scaffolds, due to their biocompatibility and extracellular matrix-mimicking porous structure, have emerged as prime candidates in this area. Moreover, their hygroscopic properties and tunable mechanical characteristics render them statishic for various tissue aminuments and intention. properties and tunable mechanical characteristics render them satiable for various tissue engineering applications. Despite their promising attributes, a significant manufacturing challenge persists: the optimization of cellular growth within the confines of lydroged scaffolds. Effective vascularization, essential for optimal cellular nutrient and oxygen supply, remains elusive. Our previous manufacturing research tackled this, introducing a novel hybrid Bio-Fabrication technique. This technique integrated coaxial electrosypinning and extrusion-based bioprinting methodologies, yielding hydroged scaffolds fortified with microtubes. These strategically embedded microtubes, modeled after capillary structures, function as microchannel diffusion conduits, enhancing cellular viability within the hydrogel marrix. A core aspect of scaffold manufacturing is ensuring the stability of its 3D architecture, especially postswelling. Preliminary hypotheses suggest a gamat of factors ensuring the stability of its 3D architecture, especially post-swelling, Preliminary hypotheses suggest a genut of factors— including microtube shape, size, orientation, alignment, and density — play determinant roles in shaping the scaffold's mechanical attributes. This research rigorously examines the mechanical evolution of hydrogel scaffolds when supplemented with aligned electrospun microtubes across a spectrum of densities. A blend of sodium alginate (SA) and gelatin was selected for the hydrogel matrix due to their inherent biocompatibility and favorable mechanical properties. Different concentrations were prepared to assess the optimal mixture for mechanical stability. A co-axial electrospinning setup was employed where polycarplactone (PCL) was used as the sheath material and polyethylene oxide (PEO) functioned as the core. This dual material approach was intended to leverage the This dual material approach was intended to leverage the structural rigidity of PCL with the biodegradability of PEO. The spinning parameters, including voltage, flow rate, and tip-to-collector distance, were meticulously adjusted to produce

aligned microrubes of varied densities and diameters. Once the microrubes were synthesized, they were layered within the hydrogel constructs. The layering process involved depositing a hydrogel layer, positioning the microrubes, and then sealing with another hydrogel layer. The entire structure was then solidified using calcium chloride, resulting in a robust, multi-layered composite. Post-fabrication, the hydrogel scaffolds underwent mechanical evaluations. Compression tests were employed to measure the compressive modulus. Tensile tests were conducted to determine ultimate tensile strength. These tests were conducted to determine ultimate tensile strength. These tests were recical to understanding the impact of microtube density on the overall mechanical properties of the hydrogel scaffolds. The high-density group, while showing improved mechanical properties over the control group, did not surpass the low-density group, suggesting a possible saturation point. In conclusion, our research methodically explored the influence of microtube density on the mechanical and structural attributes of hydrogel scaffolds. The manufacturing insights gleaned hold substantive implications, promising to propel the field of tissue engineering and drive transformative advancements in biomedical manufacturing. aligned microtubes of varied densities and diameters. Once the

nufacturing.

Keywords: Biofabrication, Electrospinning, Hydrogel, chanical Properties, Tissue Engineering.

1. INTRODUCTION

Scaffolds, a cornerstone of tissue engineering, are engineered to support cell growth both in vitro and in vivo, facilitating applications in cell therapy, organoids, and tissue regeneration processes [1]. Hydrogel scaffolds, known for their viscoclastic properties, are especially significant in soft tissue engineering, offering a versatile platform for cell culture and regeneration. They leverage decellularized extracellular matrix (ECM) for ECM hydrogel therapies and are crafted from both synthetic and natural materials to support specific cell types [2-6]. Common materials used in tissue-engineered scaffolds include Gelatin and SA, chitosan, etc. [7]. SA, owing to their cross-linking capability with divalent metallic ions like Ca³⁺, has been widely studied for viscoclastic scaffold structures with tunable material stiffness [8, 9]. Gelatin provides structural rigidity, temperature-controlled mechanical properties, and appropriate attachment ligands for cells [10-12]. appropriate attachment ligands for cells [10-12].

© 2023 by ASME

One of the key obstacles in advancing tissue engineering is the absence of functional capillaries in bioprinted tissues. Porosity alone does not ensure adequate mass diffusion, as structural changes from swelling can impede this process. Therefore, creating perfusion channels that mimic capillary vessels within the cell-laden scaffold is crucial for supporting cellular metabolism and enabling the successful construction of large-scale tissues and organs. Our previous studies have demonstrated the utility of aligned porous microtubes in enhancing cellular viability within three-dimensional (3D) hydrogel structures [13]. This approach leverages the inherent microfluidic properties of the microtubes to promote efficient exchange of nutrients and waste products between cells and the surrounding hydrogel matrix. The rationale for employing aligned microtubes lies in their ability to establish well-defined microfluidic networks throughout the biocompatible scaffold, thereby ensuring optimal fluid flow and minimizing the potential for blockages that could impede nutrient delivery and cellular function. One of the key obstacles in advancing tissue engineering is

function.

Building on this groundwork, our study investigates how microfluidic channels affect the mechanical characteristics of biofabricated scaffolds. Using core-shell electrospinning, we create biomimetic microtubular structures within Sa-gelatin hydrogels. We then conduct comprehensive mechanical testing to assess the scaffolds' response to stress. This analysis reveals the impact of the embedded microchannels on the scaffolds' stiffness, strength, and other mechanical properties, offering exited his pickle into their functionality and applicability in tiese. siffness, strength, and other mechanical properties, offering critical insights into their functionality and applicability in tissue engineering. This enhanced understanding will inform the optimization of microfluidic scaffold designs, improving their efficacy and reliability for creating advanced tissue constructs, [14]. This study is based on the hypothesis that the gradual inclusion of aligned electrospum microtubular structures would lead to modifications in mechanical characteristics, specifically in the modulus of elasticity. Additionally, we anticipate that specific interactions among the hydrogel components will induce changes in the mechanical attributes of the hydrogel framework. The primary focus of this research was to investigate and develop models that could elucidate how varying concentrations of SA and gelatin within the hydrogel impact its mechanical behavior in presence of microtubes.

Our experimental setup divided samples into three groups based on microtube content: no microtubes, low-density microtubes, and high-density aligned microtubes. This examples and interactive thin a hydrogel matrix composed of SA and gelatin, especially when enhanced with aligned microtubes. In tissue companies and the properties interact within a hydrogel matrix composed of SA and gelatin, especially when enhanced with aligned microtubes. In tissue engineering, hydrogels embedded with structures akin to capillary vessels offer considerable promise. This method represents an encouraging direction, hinging on the accurate customization of mechanical attributes to meet the unique demands and challenges of the field. Such developments could critical insights into their functionality and applicability in tissue

customization of mechanical attributes to meet the unique demands and challenges of the field. Such developments could herald significant advancements in regenerative medicine and the field of biomaterials.

2. MATERIALS AND METHODS

2.1 Materials Used

To formulate the hydrogel, SA and gelatin were employed due to their biocompatibility and ability to maintain a structural shape [15, 16]. The microtubes were crafted using polycaprolactone (PCL) and polytehylene coxide (PEO) due to their biocompatibility [17, 18]. SA, gelatin (derived from prorien skin, type A), PCL (MW = 80,000), and PEO (MW = 300,000) were procured from Sigma-Aldrich (St. Louis, MO). Calcium chloride (Anhydrous) served as the crossinking agent and was obtained from 17. Baker Chemicals, Dichloromethane (90,9%) (PCM) for the present was executed from WM. (99.9%) (DCM) for the process was acquired from VWR Chemicals (Radnor, PA).

2.2 Electrospinning process

To achieve microtubes mimicking capillary size and ensuring successful electrospinning, we selected a 12% PCL (w/v) as shell and 6% PEO (w/v) as core concentration in DCM. This choice builds upon studies like Qay et al. [19] demonstrating effective microtube formation within the desired size range of 5-20 µm. As preliminary findings indicate good cell adhesion with this ratio [13], PCL and PEO were individually dissolved in DCM at concentrations of 12% (w/v) and 6% (w/v), respectivally for our study.

arssorved in D.CM at concentrations of 12% (w/v) and 6% (w/v), respectively for our study.

Both solutions were prepared by stirring for four hours using a magnetic stirrer. The electrospinning process was executed with flow rates of 3ml/hr and 4.8ml/hr for the PEO (core) and PCL (sheath) solutions. To get aligned microtubes the working distance was maintained at 20 cm between the nozzle tip and the collector plate (comprising two parallel aluminum bars). Microtube collection took place under conditions of 65% humidity and with a 15kV applied voltage. Figure 1(a) confirms the successful alignment of the microtubes. Figure 1(a) presents an SEM image of the resulting porous electrospun microtubes. The outer diameter was measured to be approximately 3-4 μm, and the inner diameter ranged between 1.3-2 μm. Imaged software was used to quantify the porosity of the microtubes, resulting in a value of 12±2 W. The pore size distribution, also analyzed using ImageJ, spanned from 0.01 to 0.13 μm², with an average pore size of 0.043±0.025 μm².

2.3 Hydrogel Preparation

Four distinct concentrated solutions of SA and gelatin were rour atstinct concentrated solutions of SA and gelatin were prepared by dissolving them in de-ionized water, as detailed in Table 1. Each solution consisted of SA and gelatin at varying concentrations. To ensure homogeneity, mechanical stirring was employed for 5 hours, followed by sonication in a bath to eliminate any entrapped air bubbles.

TABLE 1: CONCENTRATION OF PREPARED SOLUTIONS

No.	Sodium alginate % (w/v)	Gelatin % (w/v)
1	3	3
2	6	3
3	3	6
4	6	6

Casting molds were employed for both compression and tensile testing, with distinct geometries catering to their specific purposes. Compression testing utilized cylindrical molds measuring 2.7 cm in diameter and 5 mm in thickness.

Tensile testing, requiring analysis of localized mechanical properties, used dog-bone shaped molds featuring a narrow section of 10 mm width and 7.8 mm length, flanked by wider

section of 10 mm width and 7.8 mm length, flanked by wider grip areas with a total length of 51 mm. The crosslinking within the scaffolds was facilitated by using 3% calcium chloride (w/v). Figure 2 shows the post cross-linked hydrogel scaffolds prepared by the casting process.

The process for creating hydrogel scaffolds with microtubes followed by casting process initially involves filling half of the mold with the hydrogel solution. Subsequently, a layer of microtubes is incorporated, followed by filling the remaining space in the mold with the hydrogel solution, as illustrated in Figure 3. Then, the scaffolds were soaked in CaCl₂ bath for 20 minutes each. Any excess microtubes extending beyond the edges of the samples were trimmed.

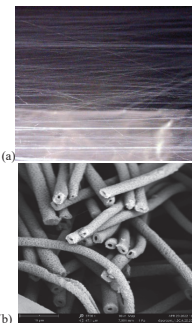


FIGURE 1 MICROTUBES CUNDER DIGITAL MICROSCOPE, WORKING DISTANCE 15 CM, MAGNIFICATION 200X), (B) MICROTUBES UNDER SCANNING ELECTRON MICROSCOPY (10 KV, WORKING DISTANCE 7.99

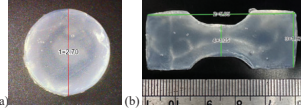


FIGURE 2: HYDROGEL SCAFFOLDS AFTER CROSS LINKING FOR (A) COMPRESSION TESTING (DIAMETER 2.7 CM), (B) TENSILE TESTING (OVERALL LENGTH 5.05 CM, OVERALL WIDTH 1.87 CM, THE NARROW SECTION WIDTH 1.05 CM)

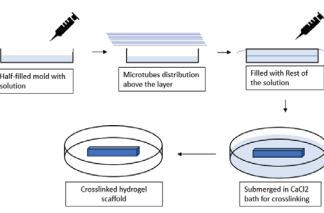


FIGURE 3: STEPS INVOLVI SCAFFOLDS WITH MICROTUBES STEPS INVOLVING MAKING HYDROGEL

2.4 Compression and Tensile Test

We conducted compression and tensile tests to investigate the mechanical characteristics and the effects of integrating microtubes into hydrogel scaffolds, considering variations in SA and gelatin concentrations.

For the unconfined compression tests, we used a microtester (MTESTQuatro®, Admet, Norwood, MA) with 5N load limit and measured the initial dimensions of the hydrogel scaffolds with a vernier caliper. During testing, the samples were placed between non-permeable plates, subjected to a constant displacement rate of 10mm/min, and given an initial preload of 0.1 N.

0.1 N.

Uniaxial tensile testing was conducted on each hydrogel scaffold using a Shimadzu AGS-X universal testing machine. Samples were aligned with the longitudinal direction of the microtubes and subjected to a constant displacement rate of 3 mm/min with a gripper separation of 2 cm shown as Figure 4. To visualize the impact of microtube integration and varying SA/gelatin concentrations on mechanical properties, data smoothing was applied via a moving average method. Acknowledging the preliminary nature of this research, only one sample per group was tested to acquire initial compression and tensile data for further investigation.

© 2023 by ASME



FIGURE 4: SCHEMATIC DIAGRAM FOR APPLIED FORCE

2.5 Data Analysis and Modelling

To investigate the impact of material concentration and electrosyum microtube density on the mechanical properties of biofabricated hydrogels, we examined the main effects of these variables. A full factorial design was created, featuring high and low levels of continuous variables—namely, gelatin and SA concentration—and three discrete levels of microtube density. Previous in vitro studies within tissue engineering have established a concentration range of 3-6% (w/v) for SA as optimal for both post-crosslinking stability and favorable cell attachment behavior [16, 20-23]. This biocompatible range promotes both hydrogel integrity and cellular function. Similarly, gelatin exhibits biocompatibility and maintains shape stability at room temperature, making it a suitable candidate for tissue engineering applications. Studies utilizing gelatin hydrogels often employ concentrations within the 3-6% (w/v) To investigate the impact of material concentration and hydrogels often employ concentrations within the 3-6% (w/v)

hydrogels often employ concentrations within the 3-6% (w/y) range [16, 24-26]. For this experiment, we established the upper limit (+) for gelatin and SA concentrations at 6% (w/v) in DI water, with the lower limit (-) set at 3% (w/v) in DI water. The three discrete microtube density levels were designated as high-density, low-density, and without microtube. For the low- and high-density groups, the microtube distribution was approximately 50-65/mm and 95-120/mm, respectively. The details of this Full Factorial design, which combines 2-level continuous and 3-level discrete factors, resulting in 12 sets of experiments, are presented in Table 2.

TABLE 2: THE DESIGN OF EXPERIMENT TABLE WITH THE CONTINUOUS AND DISCRETE VARIABLES.

Pattern	Gelatin	SA	Microtube Density
	3	3	None
0	3	3	Low
+	3	3	High
++0	6	6	Low
++-	6	6	None
++	6	3	High
+-0	6	3	Low
+	6	3	None
	3	6	None
-++	3	6	High
+++	6	6	High
-+0	3	6	Low

The gathered data on mechanical properties were then applied to fit a multiple regression model using ordinary least squares (OLS). This approach helped generate a linear predictive model based on gelatin and SA concentrations, as well as microtube density. The categorical variable (microtube Density) is used with a set of dummy or indicator variables [27] and the OLS equation is modelled with a shift [28]. The generalized model equation with the shift is shown as follows:

$$Y = \beta_0 + \beta_1 X_1 + \beta_2 X_2 + ... + \beta_i X_i + Match(X_j) \begin{cases} +1 \\ -1 & \\ else \end{cases}$$

model equation with the shift is shown as follows: $y = \beta_0 + \beta_1 X_1 + \beta_2 X_2 + ... + \beta_i X_i + Match(X_j) \begin{cases} +1 \\ -1 &(i) \\ else \end{cases}$ In the referred equation (i), β_0 is the model intercept, β_i are the coefficients associated with the predictor x_i . Match (X_j) shifts the intercept of the model equation above or below the average intercept value based on the factor match (No, Low, Highdensity microtube) [29].

3. RESULTS AND DISCUSSION

The mechanical properties of microtube-embedded hydrogel scaffolds with different SA and gelatin concentrations were assessed through compression testing. The stress-strain response of twelve distinct samples shown in Figure 5 revealed a consistent trend: scaffolds with higher microtube density consistently demonstrated greater stiffness, quantified by elevated Young's modulus values summarized in Table 3. Notably, the stress-strain curves exhibited a predominantly linear behavior within the 0-25% strain range (Figure 5). These findings suggest a significant influence of microtube density on the stiffness of hydrogel scaffolds, potentially holding implications for applications in tissue engineering and other biomedical fields. Further studies are warranted to delve deeper into the underlying mechanisms and optimize microtube design

biomedical fields. Further studies are warranted to delve deeper into the underlying mechanisms and optimize microtube design for specific applications.

In the case of Solution 2 (SA: Gelatin = 6:3), the stiffness of the scaffold without microtubes was not significantly different from that of the scaffold with low-density microtubes. However, for Solution 3 (SA: Gelatin = 3:6), the stiffness of the scaffold with high-density microtubes was notably elevated.

TABLE 3: SUMMARY OF YOUNG'S MODULUS FROM COMPRESSION TEST (UNIT IN KPA)

Micro -tube	SA:Gelatin = 3:3	SA:Gelatin = 6:3	SA:Gelatin = 3:6	SA:Gelatin = 6:6
None	43.09	20.09	30.92	34.49
Low	57.85	22.93	45.51	44.85
High	72.23	34.45	52.33	52.60

These findings contribute to our understanding of how varying microtube densities impact the mechanical characteristics of the hydrogel scaffolds under compression, essential for evaluating their potential for in vivo tissue

applications. Shift Model OLS equation for Modulus from the compression test (R2 = 64%): for the Young's

$$\begin{split} E &= 63.22 + 0.55*Gel - 5.13*Alg + \\ Match(Microtube\ Density) \begin{cases} None \rightarrow (-10.46) \\ Low \rightarrow (0.17) \\ High \rightarrow (10.28) \end{cases} \end{split}$$

Figure 6 illustrates the actual value and predicted value of modulus of elasticity for compression testing in Ordinary least squares (OLS) regression performance model.

To depict the distinct influence of each component, we constructed modulus main effect plots [30]. Figure 7 sheds light on the intricate interplay between microtube density, SA, and gelatin, and their combined influence on the elastic modulus gleaned from compression testing. A positive correlation memerges between microtube density and elastic modulus, suggesting that increasing the density of these microtubes reinforces the hydrogel structure. However, the relationship between SA and elastic modulus exhibits a more nuanced picture. Within the main plot of Figure 7, SA exhibits a negative impact on the elastic modulus across the tested range for overall shift. This trend suggests that SA might disrupt the internal network of the hydrogel, leading to decreased stiffness in the presence of gelatin. However, Table 3 reveals a non-linear this negative effect, leading to a slightly positive impact of SA on the elastic modulus. However, this positive influence remains inconsistent.

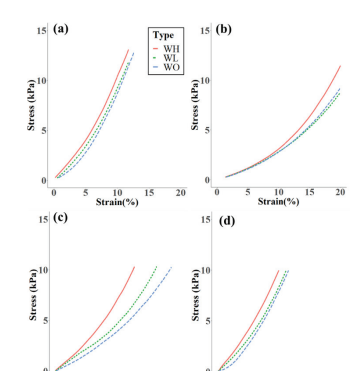
In contrast the effect of gelatin appears relatively neutral in

inconsistent.

In contrast, the effect of gelatin appears relatively neutral in Figure 7, as its effect plot displays a horizontal trend. However, Table 3 paints a more complex picture, aligning with the observations for SA. At lower gelatin concentrations, a negative impact on elastic modulus is observed, similar to SA. However, at higher gelatin concentrations, a positive impact emerges, albeit not consistent. These observations highlight the importance of considering the interplay between all three components when interpreting the effect on elastic modulus. The security of the control of the cont

components when interpreting the effect on elastic modulus. The seemingly contradictory results from Figure 7 and Table 3 underscore the need for a comprehensive understanding of the complex interactions between SA, gelatin, and microtube density. By delving deeper into these manness, we can gain valuable insights into the design and optimization of hydrogel composites with desired mechanical properties.

To assess the potential of microtube-integrated hydrogel scaffolds for in vivo applications, tensile testing was performed on samples fabricated with varying SA and gelatin concentrations. Intriguingly, the presence of microtubes consistently resulted in enhanced ultimate tensile strength (UTS) compared to pure hydrogel counterparts, as evidenced by the stress-strain curves depicted in Figure 8.



0 5 100 15 20 0 5 110 15 20 Figure 5: PLOTS OF COMPRESSION STRESS VS STRAIN FOR (A) 3% GELATIN 3% SA 3% GELATIN (B) 6% SA 3% GELATIN (C) 3% A6% GELATIN (D) 6% SA 6% GELATIN LEGENDS (WILL HIGH MICKOTUBE DENSITY, WL. LOW MICROTUBE DENSITY, WC. NO MICROTUBE

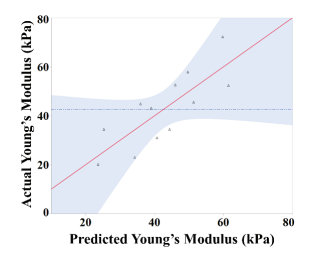


FIGURE 6: PREDICTED VS ACTUAL DATA WITH THE FIT-LINE (RED) SHOWING THE OLS REGRESSION PERFORMANCE OF MODULUS OF ELASTICITY FOR COMPRESSION TESTING

© 2023 by ASME

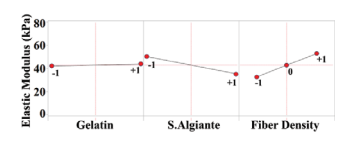


FIGURE 7: MAIN EFFECTS PLOT FOR ELASTIC MODULUS (COMPRESSION TEST) VS GELATIN, SA, AND MICROTUBE DENSITY DENSITY

Notably, within the investigated parameter range, microtube Notably, within the investigated parameter range, microtube density did not exhibit a statistically significant influence on UTS. Table 4 summarizes the observed UTS values for each scaffold composition, providing a concise overview of the tensile properties. These findings highlight the potential benefit of incorporating microtubes for improved mechanical stability in hydrogel scaffolds, warranting further exploration of the underlying mechanisms and optimization for specific in vivo amplications. applications

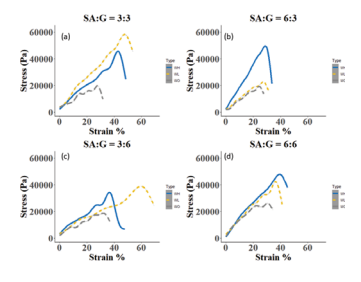


FIGURE 8: SHOWING PLOTS OF TENSILE STRESS VS STRAIN FOR (A) 3% GELATIN 3% SA (B) 6% SA 3% GELATIN (C) 3% SA 6% GELATIN (D) 6% SA 6% GELATIN. LEGENDS (WH: HIGH MICROTUBE DENSITY, WL: LOW MICROTUBE DENSITY, WO: NO MICROTUBE).

A closer analysis of ultimate tensile strength (UTS) data reveals a curious anomaly. At the lowest SA concentration (3%), both high-density microtube scaffolds exhibited lower UTS than their low-density counterparts. This deviation could be attributed to several factors: (1) lamination caused by high microtube density, (2) insufficient crosslinking time, (3) intricate intermolecular

bonding between gelatin and SA, or (4) a systematic error. tudies are crucial to validate these explanation

TABLE 4: SUMMARY OF ULTIMATE TENSILE STRENGTH FROM TENSILE TESTING (VALUES ARE IN KPa)

Type	SA:Gelatin = 3:3	SA:Gelatin = 6:3	SA:Gelatin = 3:6	SA:Gelatin = 6:6
WO	19.16	18.82	18.33	25.74
WL	57.54	22.36	40.18	40.80
WH	44.59	48.85	34.73	47.28

The shift OLS regression model equation for predicted ultimate tensile strength for this tensile testing (R²=62%):

tensile strength for this tensile testing (R2=62%):

$$UTS = 38.61 - 0.237 * Gel - 0.593 * Alg$$

$$+ Match(Fiber Density) \begin{cases} No \rightarrow (-14.35) \\ Low \rightarrow (5.36) \\ High \rightarrow (8.998) \end{cases}$$

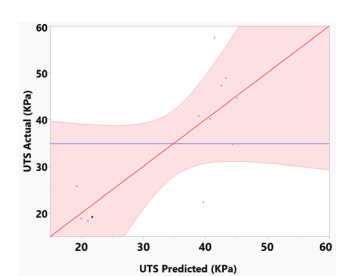
Figure 9 showcases the performance of the Ordinary Least Figure 9 showcases the performance of the Ordinary Least Squares (OLS) regression model in predicting ultimate tensile strength (UTS). The model achieves a 62% R-squared value, signifying a moderate correlation between predicted and actual UTS values. Delving deeper into the key contributors to UTS, Figure 10 explores the main effects of gelatin, SA, and microtube density. Strikingly, the prediction profiles for gelatin concentration across all outcomes in Figure 10 exhibit a relatively flat trend. This suggests that within the tested range, gelatin concentration has minimal influence on the scaffold's UTS. This observation aligns with the findings presented in Table 4, where a similar effect of gelatin on UTS is observed for scaffolds with low SA concentration (3%). scaffolds with low SA concentration (3%).

scaffolds with low SA concentration (3%).

However, a fascinating divergence emerges at higher SA concentration (6%). Table 4 reveals that increasing gelatin concentration leads to increased UTS for scaffolds without microtubes and those with lower microtube density. This contrasting behavior warrants further investigation to elucidate the underlying mechanisms governing the complex interplay between gelatin, SA, and microtube density in influencing UTS. In contrast, SA concentration demonstrates a negative effect in combination with the gelatin polymer, consistent with the main effect analysis of the modulus of elasticity in compression testing.

testing.

The prediction profile illustrated in Figure 10 for microtube density indicates an incremental relationship with UTS. As the density of microtubes increases, there is a corresponding increase in UTS. This observation adds valuable insights into the nuanced influence of gelatin, SA, and microtube density on the tensile properties of the hydrogel scaffolds, offering a comprehensive understanding of their mechanical behavior under tensile forces.



UTS Predicted (KPa)
Figure 9: PREDICTED VS ACTUAL DATA WITH THE FIT-LINE
(RED) SHOWING THE OLS REGRESSION PERFORMANCE OF
ULTIMATE TENSILE STRENGTH.

To elucidate the intricate relationships between microtube To elucidate the intricate relationships between microtube incorporation and the mechanical properties of hydrogels, our study employed Ordinary Least Squares (OLS) shift regression models. These models achieved impressive R-squared values of 64% and 62% for compression modulus and ultimate tensile strength, respectively. Notably, the strength of this approach lies in its ability to capture observed abrupt changes within the data. Unlike a single constant-slope approach, shift regression leverages individual OLS lines fitted to distinct "shift" segments, resulting in a singificantly more accurate presengation of the

leverages individual OLS lines fitted to distinct "shift" segments, resulting in a significantly more accurate representation of the complex dynamics at play. This nuanced approach sheds light on the intricate interplay between microtube incorporation and mechanical properties, paving the way for further optimization and targeted design of hydrogel materials.

While the obtained R-squared values indicate a good overall trend and successfully capture individual shifts within the data, the inherent complexity of hydrogel behavior remains evident. This complexity presents a natural limitation for shift OLS models. To account for this inherent variability and potentially improve the explanatory power of our models, future investigations will explore the influence of additional variables. These may include fabrication processes, cross-linking times, These may include fabrication processes, cross-linking times, solution concentrations, and microtube alignment direction. By incorporating these factors, we aim to achieve higher R-squared values and gain a more comprehensive understanding intricate relationships between diverse variables and the resultant mechanical properties of hydrogels.

resultant mechanical properties of hydrogels.

As depicted in Figures 7 and 10, the main effects plot reveals no statistically significant influence of gelatin concentration on either compression modulus or ultimate tensile strength (UTS). This suggests that the investigated concentration range might not have captured a region where substantial changes in mechanical properties occur. Future studies exploring a broader range of gelatin concentrations could potentially unveil concentration-

dependent trends and enhance our understanding of the

material's response.

This is particularly relevant considering the complex interplay of molecular interactions that governs the mechanical behavior of our hydrogel framework. At the core lies ionic bonding between sodium alginate's guluronic acid residues and calcium, providing a robust structural foundation [31]. Extensive calcium, providing a robust structural foundation [31]. Extensive hydrogen bonding permeates both SA and gelatin, further stabilizing the network and influencing stiffness and elasticity. Additionally, hydrophobic interactions within gelatin contribute to its stability, while chain entanglement between SA and gelatin physically restricts movement, impacting properties like viscosity and elasticity [32]. Unveiling the synergistic nature of these interactions at the molecular level holds the key to tailoring the overall mechanics of the hydrogel framework. This would allow us to optimize its behavior for specific applications, as previously demonstrated in related studies [26, 33].

The results from both compression testing and tensile testing

The results from both compression testing and tensile testing affirm the validity of our hypothesis. While the strength and modulus of elasticity for human cartilage are measured in larger units (MPa) [34], numerous internal tissues in the human body. unts (MPa) [34], numerous internal tissues in the human body, such as the uvita, soft palate itssue, base of the human tongue tissue, human tonsil tissue, esophagus, lung tissue, breast, liver, gallbladder, stomach, kidney, uterus, and others, exhibit strength in the KPa scale [35-46]. Our focused study, albeit limited in scope, serves as a steppingstone for a new avenue of research—incorporating aligned microtubes into hydrogle saffolds with the goal of rendering them suitable for eventual organ transclants. transplants.

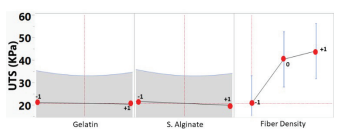


FIGURE 10: MAIN EFFECT PLOT FOR UTS AGAINST GELATIN, SA CONCENTRATION AND MICROTUBE DENSITY

This finding broadens the horizons for further research and

This finding broadens the horizons for further research and innovation within the field, especially concerning the development of scaffolds embedded with aligned fibers that are mechanically compatible with different types of fibrous human tissues. This compatibility is crucial for the success of implants or grafts in regenerative medicine, ensuring that they integrate seamlessly into the body's exiting structures.

Furthermore, this research lays the groundwork for more nuanced insights into the mechanical properties of scaffolds that are crucial for vascularization. Ensuring that the mechanical properties of scaffolds, such as elasticity and stiffness, are compatible with native tissues is vital for successful integration and functioning of the capillary networks within the body. It prompts a deeper investigation into how variations in gelatin and SA concentrations, as well as microtube densities, might be fine-

© 2023 by ASME

tuned to closely replicate the mechanical environment of specific tuned to closely replicate the mechanical environment of specific internal tissues. Understanding how the density of these microtubes affects the scaffold's properties can lead to designs that better support the formation and growth of blood vessels, essential for supplying nutrients and oxygen to the engineered tissues. In the long term, these explorations could pave the way for developments of vascularized tissues that of developments of vascularized tissues that necessary with the patient's existing vasculature.

4. CONCLUSION

In conclusion, this study sheds significant light on the intricate interplay between material concentration, microtube density, and the resulting mechanical properties of capillary-embedded hydrogel scaffolds, offering valuable insights for researchers in the field of biofabrication. Our findings provide compelling evidence that the strategic manipulation of both gelatin and SA concentrations, coupled with the careful integration of aligned microtubes within the scaffold structure, plays a pivotal role in governing the overall mechanical characteristics of these composite materials. Notably, a full factorial design approach, combined with Ordinary Least Squares (OLS) regression analysis, proved highly effective in elucidating these complex relationships, demonstrating their potential as valuable tools for future scaffold research. Importantly, our results revealed a direct correlation between increased microtube density and enhanced stiffness within the intricate interplay between material concentration, microtube increased microtube density and enhanced stiffness within the scaffolds. This finding holds significant promise for tissue engineering applications, where mimicking the mechanical properties of native tissues is crucial for promoting successful vascularization and tissue formation. For instance, in bone tissue vascularization and tissue formation. For instance, in bone tissue engineering, achieving a stiffness comparable to native bone is critical for proper integration and functionality of the implant. While our study focused on a specific concentration range, acknowledging the limitations of this scope, future investigations employing broader ranges and in vivo testing are warranted to further validate these observations and translate these findings into clinically relevant applications. Ultimately, the knowledge gained from this study transcends the realm of biofabrication, contributing to the broader field of materials science by highlighting the effectiveness of utilizing a full factorial design and OLS regression analysis to unravel the intricate relationships between composition and properties in intricate relationships between composition and properties in complex composite materials. This approach paves the way for the rational design and optimization of various materials beyond hydrogels, opening avenues for diverse applications ac various scientific and technological fields.

ACKNOWLEDGEMENTS

The authors sincerely thank Dr. Weilong Cong at Texas Tech University for providing access to the universal testing machine used in this study. This work is partially funded by NSF under grant number CMMI-2145108.

REFERENCES

- Li, W., et al., Multiple comparisons of three different sources of biomaterials in the application of tumor tissue engineering in vitro and in vivo. International journal of biological macromolecules, 2019. 130: p.
- journal of biological macromolecutes, 2019. 130: p. 166-176.

 Demirbag, B., et al., Advanced cell therapies with and without scaffolds. Biotechnology journal, 2011. 6(12): p. 1437-1435.

 Freed, L.E., et al., Advanced tools for tissue conflicts himmetatures and signaling.
- 3.
- 4.
- Freed, L.E., et al., Advanced tools for tissue engineering: scaffolds, bioreactors, and signaling. Tissue engineering, 2006. 12(12): p. 3285-3305.

 Kaur, S., et al., Non-matriged scaffolds for organoid cultures: Cancer Letters, 2021. 504: p. 58-66.

 Keane, T.J., LT. Swinchart, and S.F. Badylak, Methods of tissue decellularization used for preparation of biologic scaffolds and in vivo relevance. Methods, 2015. 84: p. 52-34.

 Remuzzi, A., et al., Experimental evaluation of kidney regeneration by organ scaffold recellularization. Scientific reports, 2017. 7(1): p. 43502.

 Zartf, M.-E., A review of chitosum, alginate-, and gelatin-based biocomposites for bone tissue engineering. Biomater. Tissue Eng. Bull, 2018. 5(3): p. 4. 5.

- Wands, I., D. Shepherd, and D. Hukins, Viscoelastic properties of composites of calcium alginate and hydroxyapatite. Journal of Materials Science: Materials
- hydroxyapatite, Journal of Materials Science: Materials in Medicine, 2008. 19(6): p. 2417-2421.
 Shi, P., A. Laude, and W.Y. Yeong, Investigation of cell viability and morphology in 3b bio-printed aliginate constructs with unable stiffness. Journal of Biomedical Materials Research Part A, 2017. 105(4): p. 1009-1018.
 C Echave, M., et al., Gelain as biomaterial for tissue engineering. Current pharmaceutical design, 2017. 23(24): p. 3567-3584.
 Janmaleki, M., et al., Role of temperature on bio-printability of gelatin methacryloyl bioink in two-step cross-linkine strateev for tissue enemieering.
- cross-linking strategy for tissue engineering applications. Biomedical Materials, 2020. 16(1): p. 015021
- 12. Ito, A., et al., Transglutaminase-mediated gelatin matrices incorporating cell adhesion factors as a biomaterial for tissue engineering. Journal of bioscience and bioengineering, 2003. **95**(2): p. 196-
- 199.
 Zhang, N., et al., Biomimetic hydrogel scaffolds embedded with porous microtubes as perfusion channels Manufacturing Letters, 2023. 35: p. 184-193. Yarin, A., Coaxial electrospinning and emulsion electrospinning of core-shell fibers. Polymers for Advanced Technologies, 2011. 22(3): p. 310-317. Wu, Z., et al., In vitro and in vivo biocompatibility evaluation of a 3D bioprinted gelatin-sodium

- alginate/rat Schwann-cell scaffold. Materials Science and Engineering: C, 2020. 109: p. 110530. Mondal, A., et al., Characterization and printability of Sodium alginate-Gelatin hydrogel for bioprinting NSCLC occulture. Scientific reports, 2019. 9(1): p. 19914.
- K., Remya, K., et al., Hybrid polycaprolactone/polyethylene oxide scaffolds with tunable fiber surface morphology, improved hydrophilicity and biodegradability for bone itssue engineering applications. Journal of Biomaterials science, Polymer edition, 2018. 39(12): p. 1444-1462. It, Y-E, et al., Ultraporous nanofeatured PCL-PEO microfibrous scaffolds enhance cell infiltration, colonization and myofibroblastic differentiation. Nanoscale, 2015. 7(36): p. 14898-14995.

 Qavi, 1. and G. Tan, Process control of electrospinning artificial fenetstrated capillary vessels. Materials & et al., Hybrid 17. Remya,
- artificial fenestrated capillary vessels. Materials & Design, 2023. 227: p. 111708. Huang, Y., et al., Nanofiber-reinforced bulk hydrogel:
- 20. preparation and structural, mechanical, and biological properties. Journal of Materials Chemistry B, 2020.
- 21.
- regeneration. Composites Part B: Engineering, 2022. 243- p. 110162. Rezaei, H., et al., In-vitro cellular and in-vivo investigation of accorbic acid and β-glycerophosphate loaded gelatin/sodium alignate injectable hydrogels for urinary incontinence reatment. Progress in Biomaterials, 2021. 10(2): p. 161-171.
- Biomaterials, 2021. 10(2): p. 161-171.

 Liu, S., et al., Sodium aliginate/collagen composite
 multiscale porous scaffolds containing poly (ecaprolactone) microspheres fabricated based on
 additive manifacturing technology. RSC advances,
 2020. 10(64): p. 39241-39250.

 Samp, M.A., N.C. Iovanac, and A.J. Nolte, Sodium
 aliginate toughening of gelatin hydrogels. ACS
 Biomaterials Science & Engineering, 2017. 3(12): p.
 3176-3182.
- 24.
- Biomaterials Science & Engineering, 2017. 4(12): p. 3176-3182.
 Saariai, A., et al., On the development and characterisation of crosslinked sodium alignate/gelatine hydrogels. Journal of the mechanical behavior of biomedical materials, 2013. 18: p. 152-166.
 Derkach, S.R., et al., Interactions between gelatin and sodium alignate: UV and FTIR studies. Journal of Dispersion Science and Technology, 2019.
 Hardy, M.A., Regression with dummy variables. Vol. o3. 1903: Sacs.
- 93. 1993: Sage. Kulendran, N. and S.F. Witt, Cointegration versus least
- 28.
- Kulendran, N. and S.F. Witt, Cointegration versus least squares regression. Annals of Tourism Research, 2001. 28(2): p. 291-311. Suits, D.B., Use of dummy variables in regression equations. Journal of the American Statistical Association, 1957. 52(280): p. 548-551.

- Keppel, G. and T. Wickens, Design and Analys Researcher's Handbook. 4th edn. Chap. 6. 2004, Pearson Education: Upper Saddle River, NJ. Mackie, W., R. Noy, and D. Sellen, Solution properties of sodium alginate. Biopolymers: Original Research on
- of sodium alginate. Biopolymers: Original Research on Biomolecules, 1980. 19(10): p. 1839-1860. Takei, T., et al., Hydrophobically-modified gelatin hydrogel as a carrier for charged hydrophilic drugs and hydrophobic drugs. International journal of biological macromolecules, 2020. 149: p. 140-147. Razzak, M.A., M. Kim, and D. Chung, Elucidation of aqueous interactions between fish gelatin and sodium alginate. Carbohydrate Polymers, 2016. 148: p. 181-188.
- 188.
 Grellmann, W., et al., Determination of strength and deformation behavior of human cartilage for the definition of significant parameters. Journal of Biomedical Materials Research Part A: An Official Journal of The Society for Biomaterials, The Japanese Biomedical Materials Research Part A: An Official Journal of The Society for Biomaterials, The Japanese Society for Biomaterials and the Korean Society for Biomaterials and the Korean Society for Biomaterials, 2006. 78(1): p. 168-174. Haddad, S.M.H., et al., Estimation of the Young's moduli of fresh human oropharyngeal soft itssues using indentation testing, Journal of the Mechanical Behavior of Biomedical Materials, 2018. 86: p. 352-358. Birch, M. and P. Srodon, Biomechanical properties of Biomedical Materials, 2018. 86: p. 352-358. Birch, M. and P. Srodon, Biomechanical properties of he human soft palate. The Celf Palate-Craniofacial Journal, 2009. 46(3): p. 268-274. Huang, Y., D.P. White, and A. Malhotra. Use of computational modelling to predict responses to upper airway surgery in obstructive sleep apnea. The Laryngoscope. 2007. 117(4): p. 648-653. Singh, G. and A. Chanda, Mechanical properties of whole-body soft human tissues: A review. Biomedical Materials, 2021. 16(6): p. 062004. Yang, J., et al., Shear modulus of elasticity of the esophagus. Annals of biomedical engineering, 2004. 32: p. 1223-1230. Polio, S.R., et al., Cross-platform mechanical characterization of Jung tissue. PloS one, 2018. 13(10): p. e0204765. Baah-Dwomoh, A., et al., Mechanical properties of female reproductive organs and supporting connective tissues: a review of the current state of knowledge. Applied Mechanics Reviews, 2016. 68(6): p. 060801. Snedeker, J.G., et al., Strain-vate dependent material properties of the porcine and human kidney capsule.

- 38.
- 39.
- 40

- Applied Mechanics Reviews, 2016. 68(6): p. 060801. Snedeker, 1.6., et al., Strain-area dependent material properties of the porcine and human kidney capsule. Journal of biomechanics, 2003. 38(5): p. 1011-1021. Lim, Y.-J., et al., In situ measurement and modeling of biomechanical response of human cadaveric soft issues for physics-baxed surgical simulation. Surgical endoscopy, 2009. 23: p. 1298-1307. Karimi, A., A. Shojaci, and P. Tehrani, Measurement of the mechanical properties of the human gallbladder.

© 2023 by ASME

- Journal of medical engineering & technology, 2017.
- Journal of medical engineering & technology, 2017. 41(7): p. 541-545. Nava, A., et al., Evaluation of the mechanical properties of human liver and kidney through aspiration experiments. Technology and Health Care, 2004. 12(3): p. 269-280. Evans, D.W., et al., Scale-dependent mechanical properties of native and decellularized liver tissue. Biomechanics and modeling in mechanobiology, 2013. 12: p. 569-580.